Global and Planetary Change 207 (2021) 103652

Contents lists available at ScienceDirect

Global and Planetary Change

journal homepage: www.elsevier.com/locate/gloplacha

Research article

Tracking magmatism and oceanic change through the early Aptian Anoxic Event (OAE 1a) to the late Aptian: Insights from osmium isotopes from the westernmost Tethys (SE Spain) Cau Core

Rafael Martínez-Rodríguez [a,*], David Selby [b,c], José M. Castro [a], Ginés A. de Gea [a], Luis M. Nieto [a], Pedro A. Ruiz-Ortiz [a]

[a] Jaén University, CEACTEMA and Geology Department, Campus Universitario, 23071 Jaén, Spain
[b] Department of Earth Sciences, Durham University, Durham DH1 3LE, UK
[c] State Key Laboratory of Geological Processes and Mineral Resources, School of Earth Resources, China University of Geosciences, Wuhan 430074, Hubei, China

ARTICLE INFO

Editor: Dr. Haywood Alan

Keywords:
Re—Os isotopes
OAE 1a
Aptian
Large Igneous Province
Western Tethys
$\delta^{13}C$

ABSTRACT

Some of the major Carbon cycle perturbations of the Phanerozoic occurred during the Aptian, in relation to magmatism. The highest temperatures reconstructed for the Cretaceous Period correspond to the Oceanic Anoxic Event of the early Aptian (OAE 1a), an episode of accelerated global change. Here we present a chemostratigraphic study based on osmium isotopes integrated with high-resolution Carbon-Oxygen stable isotope data from the Cau Core (Western Tethys, SE Spain), including a 6.4 Ma record from the early to the late Aptian. This high-resolution study of the continuous and expanded Cau section permits a thorough understanding of the duration of the Aptian events, as well as an evaluation of the mechanisms triggering the abrupt changes of the global carbon and osmium cycles and their interdependence. Here we show that the Large Igneous Province (LIP) Aptian magmatism initiated 550–750 kyr prior to the OAE 1a, and persisted for 1.4 Myr after the event, influencing the composition of seawater for 2.8 Myr. We show a continuous Os isotope record encompassing the OAE 1a and the late Aptian for the first time, and demonstrate that the recovery from the exceptionally unradiogenic composition of seawater Os produced by the dominance of the Ontong Java Plateau volcanism, was slow. Our results demonstrate the different time duration of some events, and the asynchronous relationship between the carbon and osmium cycles

1. Introduction

The Aptian (121.4–113.2 Ma, Gradstein et al., 2020), records major environmental perturbations at both global and local scales, reflected in prominent climatic changes and biotic turnovers both in continental and marine realms. Also, profound perturbations in various geochemistry cycles occurred, especially in the carbon cycle (Hay, 2017; Skelton, 2003; Skelton and Gili, 2012)(; ; . The most remarkable environmental changes during the Aptian are related to the early Aptian Oceanic Anoxic Event or OAE 1a (Schlanger and Jenkyns, 1976; Arthur et al., 1990). This major event was marked by intense global palaeoclimatic and palaeoceanographic change, related to a rise in temperature that led to a hyperthermal event, increased marine productivity, depleted oxygen conditions in the oceans and widespread burial of organic matter in deep marine settings in a global context of sea-level rise (e.g., Weissert and Bréheret, 1991; Erba, 1994; Erba and Tremolada, 2004; Erbacher et al., 1996; Weissert et al., 1998; Leckie et al., 2002; Jenkyns, 2010; Erba et al., 2015; Castro et al., 2019). The OAE 1a is linked to a dramatic perturbation of the global carbon cycle reflected in a prominent negative Carbon Isotope Excursion (CIE), followed by a long-lasting positive excursion, recorded in both continental and marine domains (e.g. Menegatti et al., 1998; Erba et al., 1999, 2015; Jahren et al., 2001; Bellanca et al., 2002; van Breugel et al., 2007). The carbon cycle perturbation was triggered by massive inputs of ^{13}C-depleted carbon to the atmosphere-marine system, responsible for the negative CIE. The sources of carbon have been the subject of intense debate, and are considered to originate from different and possibly complementary sources: submarine volcanic degassing mostly from the Ontong-Java Plateau (OJP), methane emissions, and carbon emissions caused by the injection of magma into organic-rich sediments in the High Artic

* Corresponding author.
E-mail address: rodrigue@ujaen.es (R. Martínez-Rodríguez).

https://doi.org/10.1016/j.gloplacha.2021.103652
Received 9 February 2021; Received in revised form 2 September 2021; Accepted 20 September 2021
Available online 29 September 2021

Large Igneous Province (HALIP), (Adloff et al., 2020; Erba et al., 2010, 2015; Leckie et al., 2002; Méhay et al., 2009; Naafs et al., 2016; Percival et al., 2021; Polteau et al., 2016; Tejada et al., 2009; Weissert and Erba, 2004)(; ; ; ; ; ;). Although these sources are not exclusive between them, most studies agree that volcanism was the major source, while the relative role and timing of each one remains elusive.

The emplacement of Large Igneous Provinces (LIPs) led to an exceptionally massive outpouring of basalts, introducing an excess of CO_2 into the atmosphere-ocean system (e.g., Jones and Jenkyns, 2001). Causal linkages between LIPs and the OAEs have been previously proposed (e.g., Kerr, 1998; Larson and Erba, 1999; Snow et al., 2005; Kuroda et al., 2007; Turgeon and Creaser, 2008; Erba et al., 2015; Matsumoto et al., 2020). The largest estimated volcanic event in the last 200 Myr (Tarduno et al., 1991; Neal et al., 2008), the emplacement of the OJP in the central Pacific Ocean, is considered the main trigger of widespread climatic/oceanographic changes at the time of OAE 1a (Bottini et al., 2012; Erba et al., 2015; Jones and Jenkyns, 2001; Larson and Erba, 1999; Percival et al., 2021; Tejada et al., 2009; ; ; ; ;).

Starting in the earliest Aptian time, massive eruptions associated with the formation of the Greater Ontong Java Event (GOJE) (Taylor, 2006), that includes the OJP, Manihiki Plateau (MP), and Hikurangi Plateau (HP) (Chandler et al., 2012), are related to a shift in seawater osmium ($^{187}Os/^{188}Os$) isotope composition to less radiogenic values (Tejada et al., 2009). Similarly, volcanic eruptions are linked to temporal variations in sedimentary Pb isotopic values from the Tethys and Pacific oceans during the late Barremian-early Aptian interval (Kuroda et al., 2011). The GOJE, with an almost exclusively submarine character (Mahoney et al., 2001), induced warming over a long-time scale (~4 Myrs., Erba et al., 2015), producing an event of global change affecting the ocean chemistry (Kuroda et al., 2011), sedimentary and biotic processes, and thus the biomass in both marine and continental environments (Erba et al., 2015). The fluctuating intensity of GOJE volcanism produced short- and long-term temperature changes through the latest Barremian – early Aptian time interval, but the general trend indicates that global warming marked the OAE 1a (Jenkyns, 2003). The introduction of unradiogenic $^{187}Os/^{188}Os$ and nutrients to the ocean from the OJP would have been instantaneous due to the submarine character of the OJP (Kuroda et al., 2011). In contrast, mostly in the late Aptian, the Southern Kerguelen Plateau (SKP, Kerguelen LIP construction) was mainly subaerial (Frey et al., 2003), and the volcanic ash and gases were ejected into the atmosphere, inducing transient climate cooling (Bottini et al., 2015).

The termination of the OAE 1a correlates with the end or reduction of the main volcanic episode of the Ontong-Java Plateau (Tejada et al., 2009; Bottini et al., 2012) and a prominent global cooling (Bottini et al., 2015; Naafs and Pancost, 2016) linked to a reduction in the atmospheric CO_2 concentrations (Naafs et al., 2016).

The late Aptian witnessed an overall reduction in global temperatures. Although no major environmental perturbations occurred, a remarkable long-lasting negative-positive trend is recorded in the carbon isotope values, reflecting a global perturbation in the carbon cycle (e.g., Leckie et al., 2002; Erba et al., 2015; Castro et al., 2021). Neither major anoxia nor widespread organic matter deposition took place during the late Aptian, although a fall in global temperatures have been proposed (McAnena et al., 2013; Erba et al., 2015; O'Brien et al., 2017; Bottini and Erba, 2018). Volcanism at the Greater Ontong Java Event (GOJE) and the Kerguelen Plateau (KP) remained active during the late Aptian (Erba et al., 2015), whereas no direct evidence for their possible impact in the global carbon cycle has been demonstrated.

The marine Os-isotope record is considered to be a proxy for the relative inputs from continental weathering, mantle-derived volcanic and hydrothermal materials, and cosmogenic sources (Peucker-Ehrenbrink and Ravizza, 2000). Mantle and cosmogenic materials are unradiogenic ($^{187}Os/^{188}Os$ values of 0.12–0.13, (Allègre and Luck, 1980), whereas continental sources are radiogenic, with $^{187}Os/^{188}Os$ values of 1.0–1.5 (e.g., Peucker-Ehrenbrink and Ravizza, 2000).

1.1. The Cau section and study aims

Here we present a new osmium isotope record from the Cau core in Southern Spain (Castro et al., 2021), embracing the lower to upper Aptian succession, which provides further evidence for the OAE 1a interval, and represents the first study of osmium isotopes ($^{187}Os/^{188}Os$) from the late Aptian. We further discuss the links of the volcanism and other possible sources of $\delta^{13}C$ depleted carbon during the OAE 1a, and for the first time provide evidence to discuss the possible links of volcanism, carbon cycle perturbations and environmental changes during the late Aptian.

The position of Cau during the Aptian corresponds to a palaeolatitude of 20°–25° N (Masse et al., 1993) within the northern part of the arid equatorial belt (Chumakov et al., 1995) (Fig. 1). Palaeographically, active LIPs during the Aptian, such as the GOJE (including OJP, MP, and HP) in the SW Pacific ocean, and the Kerguelen Plateau, were at a very distal position from Cau, thereby, the palaeoceanographic setting of Cau is ideal to test the global character of the effects from these volcanic eruptions. Additionally, Cau is located strategically in the westernmost corridor between the Central Atlantic and the Tethys (Fig. 1). In the context of the Aptian rifting, the outer-shelf depositional setting (e.g., Martín-Chivelet et al., 2002, 2019; Vera, 2004; Castro et al., 2021) resulted in an expanded and continuous section at Cau, which permits the study of abrupt events that occur in short periods of time.

Key goals of this study include the precise timing of LIP magmatic activity due to plateau emplacements, and further insights into the time and causal links between volcanism and environmental perturbations during and after OAE 1a. A LIP association with the OAE 1a has been previously investigated using Os-isotopes ($^{187}Os/^{188}Os$) stratigraphy from four sections (Gorgo a Cerbara, Italy; Tejada et al., 2009; Cismon, Italy; DSDP Site 463, Mid Pacific Mountains; Bottini et al., 2012; Poggio Le Guaine Core; (Percival et al., 2021)). All sites record a deep oceanic palaeosetting, yet, the previously studied OAE 1a sections for Os-isotope stratigraphy do not penetrate further into the Aptian, in contrast to this study. The main objective of the study is to characterize with the highest precision the Os-isotope variations observed in the record, and to analyze them in combination with the available stratigraphic framework (C-isotopes, biostratigraphic data, total organic carbon content). The analysis of this interval embraces a detailed characterization of the Re—Os data shortly prior and during the whole OAE 1a, and long after this event for the most part of the late Aptian.

2. The CAU Core

The Cau hill (38.70389°N 0.00472°W) is located in the NE of Alicante Province, southeastern Spain. The studied lithologic interval comprises the Almadich Formation (Fm), ranging from the lowermost Aptian to the upper Aptian. The Almadich Fm lies on a discontinuity surface with a hiatus embracing the Barremian-Aptian transition, developed on the upper Barremian hemipelagic marls and marlstones of the Los Villares Fm, and it is overlain by the shallow platform carbonates of the Seguilí Fm of latest Aptian-earliest Albian age (Castro et al., 2008) (Fig. 2). The Almadich Fm was deposited in a ramp type distal marine platform, under hemipelagic conditions, located in the Southern Iberian Continental Margin (Fig. 3). Regionally, the Almadich Fm has heterochronous base and top, and is overlying a platform-drowning surface in several outcrops in Sierra Mariola and Sierra Seguilí (Castro et al., 2008; Skelton et al., 2019).

The Cau record includes a continuous expanded section that ranges from the basal Aptian (below the level of the nannoconid crisis, NC) up to the mid-upper Aptian. A quantitative study of nannofossils was performed on Cau core samples in order to establish the relative proportions of the different taxa and to locate, as reliably as possible, the "nannoconid crisis". The definition of the NC has been made following the work by Erba (1994). A decrease in *Nannoconus* ssp. relative abundance and the absence of narrow-canal nannoconid allows characterizing the

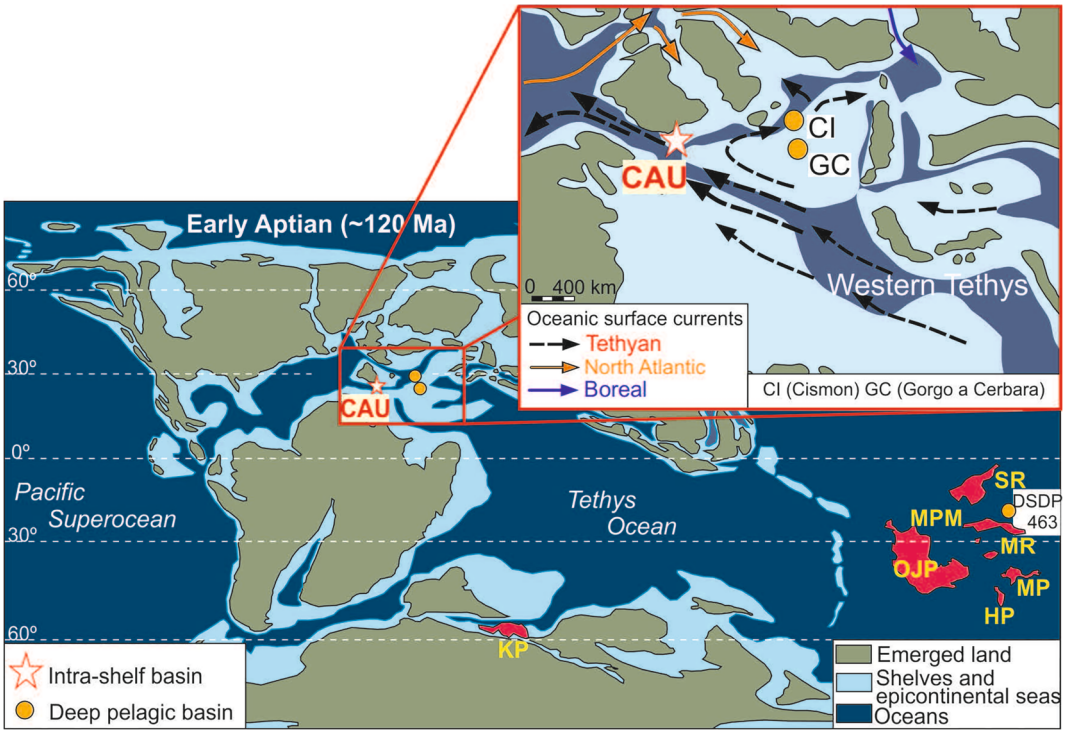

Fig. 1. Palaeogeographic maps showing the distribution of oceans and land in the Early Cretaceous (~120 Ma), and a close-up for the Western Tethys – North Atlantic corridor (Betic Seaway). Modified after Dercourt et al. (2000), Blakey (2005), Aguado et al. (2018) and Castro et al. (2021). Oceanic surface currents after Melinte and Mutterlose (2001) and Misumi and Yamanaka (2008). The location of Cau and other sites cited in the text and figures, are shown. The names of the Western Tethys successions represented by filled circles and stars on the global map are shown on enlarged map, to the left. HP: Hikurangi Plateau; KP: Kerguelen Plateau; MP: Manihiki Plateau; MPM: Mid-Pacific Mountains; MR: Magellan Rise; OJP: Ontong Java Plateau; SR: Shatsky Rise.

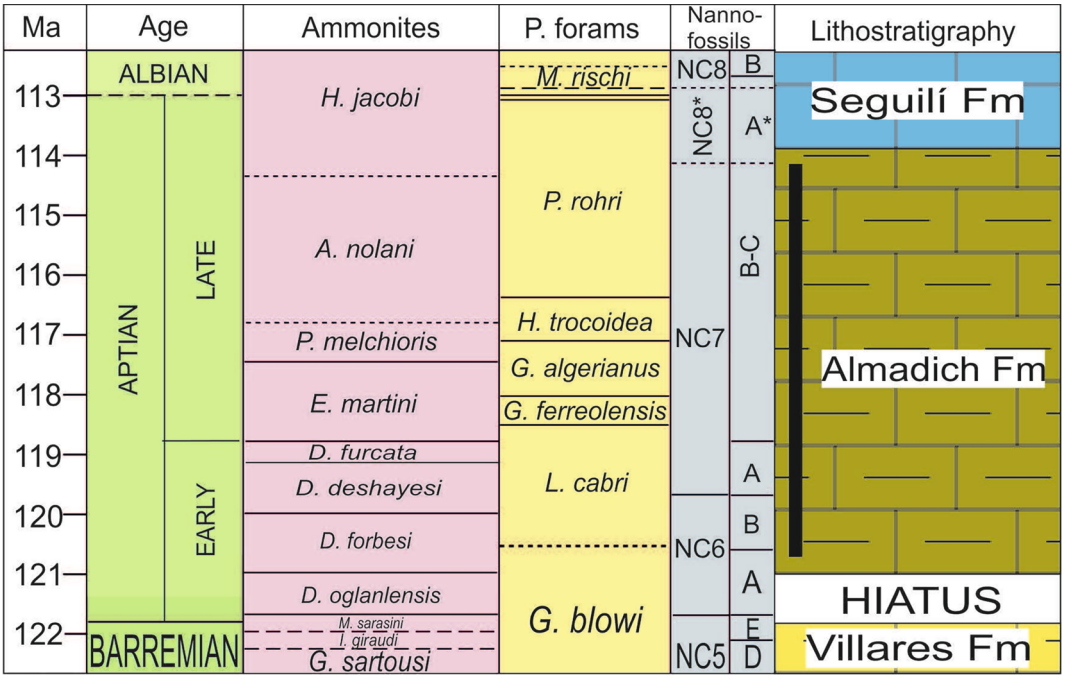

Fig. 2. Chronostratigraphic chart of the latest Barremian, Aptian and earliest Albian in Cau outcrops (province of Alicante, Spain). Time scale after Malinverno et al. (2012) and Martinez et al. (2020). The Cau Core is represented by the black vertical bar, interval of materials in this study.

"nannoconid crisis". Minima in nannoconid percentages correspond to lower part of OAE 1a. In the upper Aptian, only the wide-canal nannoconids recover and reach percentages up 15–25%. The Cau core is well constrained by calcareous nannofossil biozones NC6 (lower Aptian), NC7A (lower–upper Aptian transition), and NC7BC (lower Aptian). Planktonic foraminifera zones present in the Cau Core are *Globigerinelloides blowi* and *Leupoldina cabri* (lower Aptian), and *Globigerinelloides ferreolensis*, *Globigerinelloides algerianus*, *Hedbergella trocoidea* and

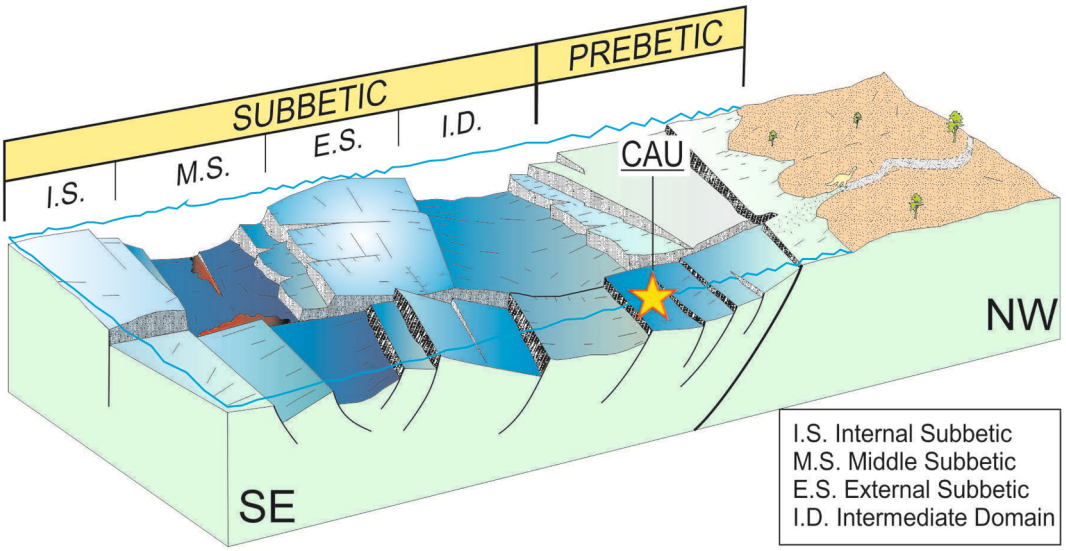

Fig. 3. Palaeogeographic reconstruction of the tectonosedimentary context for the Southern Iberian Continental Margin during the early Aptian (modified from Ruiz-Ortiz, 2010). The Cau outcrops are located in hemipelagic environments of the prebetic platform.

Paraticinella rohri (lower Aptian; Fig. 2). This biostratrigraphy correlates with the Cau Section ammonite biozones of *Deshayesites forbesi* and *Deshayesites deshayesi* (lower Aptian), and *Dufrenoia furcata* and *Epicheloniceras martini* (lower Aptian; Fig. 2).

The whole Almadich Fm is composed of hemipelagic deposits consisting of an alternating sequence of marls/marlstones dominated by mudstones/wackestones. Detailed analysis of the core recognizes five facies types: (I) dark grey massive facies; (II) light grey bioturbated facies, with Chondrites, Planolites, and other feeding, resting and undefined traces; (III) dark grey undisturbed mudstones with planar lamination; (IV) light to dark grey brecciated to nodular facies with chaotic organization; (V) grey to orange, weathered, recrystallized or altered facies.

Previously published $\delta^{13}C$ and TOC data (Castro et al., 2021) is included in this study to further discuss the Os-isotope results. The carbon-isotope values obtained are typical for Aptian hemipelagic and pelagic marlstones and limestones (Herrle, 2004; Lorenzen et al., 2013) , with $\delta^{13}C_{carb}$ values ranging from 0.67 to 4.66‰. TOC contents reach a maximum of 2% wt, with higher contents coinciding with the dark grey levels (facies Types I and III).

The age model of the Cau core has been accurately established, based on the integration of biostratigraphy (calcareous nannofossils, planktonic foraminifera and correlation with the field section ammonite data), and C-isotope stratigraphy, leading to a subdivision into 14C-isotope segments (Castro et al., 2021). The $\delta^{13}C_{carb}$ profile of the Cau Core has been precisely correlated with several records worldwide, as the section contains an excellent preserved original sedimentary signature, which makes it suitable for stratigraphic correlation (Castro et al., 2021).

The numerical model of the Cau section for this study is based on the chronology of Malinverno et al. (2012) coupled with biostratigraphy databases in reference to the Geologic Time Scale 2020 (Gradstein et al., 2020) and the recent age estimates for the Barremian-Aptian boundary (123.4–121.2 Ma; Olierook et al., 2019; and 121.40 ± 0.34 Ma; Martinez et al., 2020). The Cau core time interval ranges from 120.6 (uppermost part of *Globigerinelloides blowi* zone) to 114.2 Ma (upper part of *Paraticinella rohri* zone). Magnetostratigraphy data are no available for Cau, and there is a regional hiatus embracing the Barremian-Aptian boundary. As such, this hampers the ability to anchor an absolute age constraint for the Cau section. At Cismon, the absolute age for the base of Selli level is considered as 120.21 ± 0.04 Ma, with the nannoconid crisis cyclostratigraphically determined to have started 33 kyrs before (Malinverno et al., 2010). Alternatively, the base of the Selli level is placed between 120.70 and 120.80 Ma (Bottini et al., 2015), and the start of the nannoconid crisis estimated at 120.34 Ma (Erba, 2004). With a time range of 6.4 Myr and 144.4 m of thickness, the overall average sedimentation rate calibrated for the Cau core is 2.26 cm/kyr.

3. Analytical protocols

To provide an Os-isotope record for the entire Cau section, 56 samples were collected, between the base and top of the Cau section (144.2–6.2 m depth – core stored at Department of Geology of Jaén University). The average sample spacing was 2.6 m, although higher resolution sampling was applied to C-isotope segments Ap2, Ap3, and Ap4 (Fig. 4). Each sample (~20 g) represents a 2 cm stratigraphic interval. Prior to powdering, samples were washed with distilled water, and polished using a diamond polishing wheel to remove drill and saw marks. Samples were dried at 50 °C overnight, prior to powdering using a RM 200 agate mortar mill. The rhenium-osmium (Re—Os) analysis were undertaken in the Department of Earth Sciences, Laboratory for Source Rock and Sulfide Geochronology and Geochemistry, and Arthur Holmes Laboratory at the Durham Geochemistry Center, Durham University (UK).

To isolate the hydrogenous Re—Os fraction from the organic-rich sedimentary samples, a CrO_3–sulphuric acid digestion medium was applied (method described by Selby and Creaser, 2003). Whole rock powders (~1 g) together with a known amount of a mixed $^{185}Re+^{190}Os$ tracer solution were reacted with 8 mL of 4 N H_2SO_4 with 0.25 g CrO_3 per mL of 4 N H_2SO_4 in sealed carius tubes at 220 °C for 48 h. Osmium was extracted and purified using $CHCl_3$ solvent extraction, followed by CrO_3–H_2SO_4–HBr microdistillation.

Rhenium was isolated and purified from the CrO_3–H_2SO_4 Os extracted solution using 5 N NaOH-acetone solvent extraction, and further purified using modified HCl–HNO_3 anion bead chromatography (Selby and Creaser, 2003).

The purified Os and Re fractions were loaded onto Pt and Ni filaments, respectively. Both, Re and Os isotopic measurements were determined using a ThermoScientific TRITON mass spectrometer using static Faraday collection for Re and secondary electron multiplier in peak-hopping mode for Os. Total procedural blanks during this study were 15.0 ± 1.0 for Re, and 0.08 ± 0.05 for Os, (1σ S.D., $n = 8$) with an average $^{187}Os/^{188}Os$ value of 0.20 ± 0.05 (n = 8).

The initial $^{187}Os/^{188}Os$ composition (Os_i) at the time of deposition

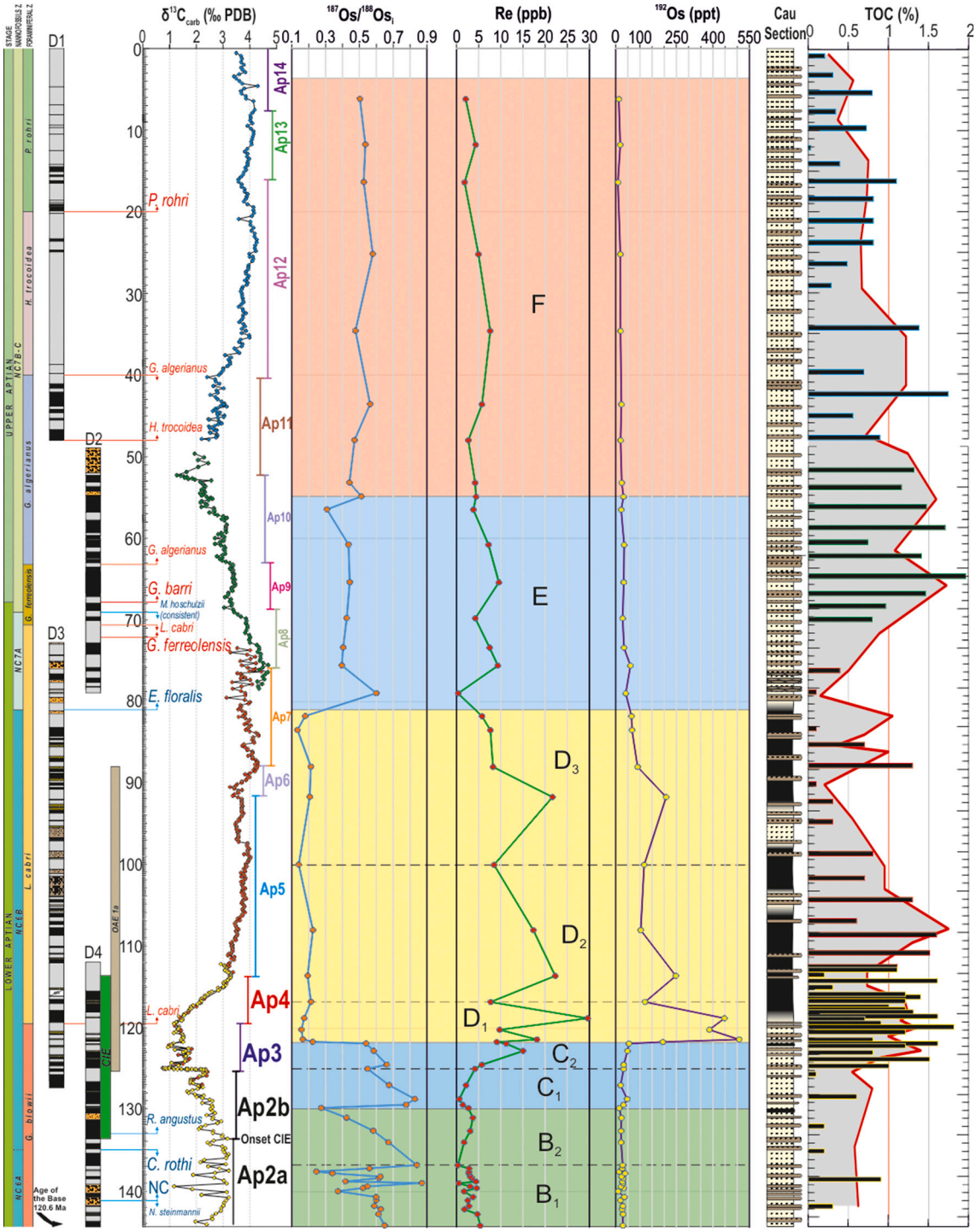

Fig. 4. Record of the Almadich Fm (D1 to D4 cores) from Cau. Stratigraphic profiles of $\delta^{13}C$ data, TOC (dots and bars in yellow – D1, red – D2, green – D3, and blue – D4) (Castro et al., 2021), Os isotope ratio, Re, and ^{192}Os concentrations are shown. Biostratigraphy (blue arrows are calcareous nannofossils, red arrows are planktic forams) zonation is from Castro et al. (2021). The outcrop section (Naafs et al., 2016) and C-intervals proposed by Castro et al. (2021), have been followed. Nanno-Nannofossils, Foram.-Foraminifera, NC-nannoconid crisis, CIE-Carbon Isotope Excursion. (For interpretation of the references to colour in this figure legend, the reader is referred to the web version of this article.)

were calculated using the equation:

$$^{187}Os/^{188}Os_{initial} = {}^{187}Os/^{188}Os_{measured} - \left[{}^{187}Re/^{188}Os_{measured} * (EXP(\lambda * t) - 1)\right]$$

where λ is the ^{187}Re decay constant = $1.666e^{-11}a^{-1}$ (Smoliar et al., 1996), and t is the depositional age given in years.

4. Results

The Os_i profile has been subdivided into 5 segments (B to F), following previously defined segments (A to E; Bottini et al., 2012), for the OAE 1a interval, adding a division in segments B and C, and a new segment F extending up to the upper Aptian (Fig. 4).Overall, the Re and ^{192}Os abundances of the 56 samples range from 0.37 to 29.63 ppb and

9.23 to 508.01 ppt, respectively (see Appendix A; Table 1; Fig. 4), with Os_i compositions ranging from non-radiogenic (0.13) to radiogenic (0.87). Segment B is divided into B_1 and B_2. Subsegment B_1 predates the OAE 1a and records the onset of the NC. In segment B_1 (base of the record to 137 m coinciding with the lower part of $\delta^{13}C$ segment Ap2) the Os_i values begin steady at ~0.60, but, at the onset of the nannoconid crisis (here defined by the Highest Occurrence, HO, of *N. steinmannii*) the Os_i describe a zig-zag profile with values between 0.24 and 0.87. This zig-zag pattern is also recorded in the $\delta^{13}C$ data (Fig. 4)In subsegment B_2 (137 to 130 m – middle part of $\delta^{13}C$ zone Ap2), the Os_i values show a gradual shift towards non-radiogenic values, from 0.84 to 0.27, which is paired with a slight increase in Re content from 0.37 to 3.76 ppb (Fig. 4), and this correlates with the onset of the C-isotope CIE predating the OAE 1a. Segment C ranges from 130 to 122 m (coinciding with the transition between C-isotope segments Ap2 and Ap3), and is divided in two subsegments C_1 and C_2. The base of C_1 is marked by an abrupt Os_i rise from 0.27 to 0.78–0.83, followed by a decrease down to 0.55, coinciding with the base of the Ap3 segment, and therefore the $\delta^{13}C$ defined base of the OAE 1a. In C_2, from the Os_i of 0.55, the values increase and fall gradually to 0.53, and then fall abruptly to a non-radiogenic Os_i value of 0.17, in the middle of Ap3 and coeval to a negative peak in $\delta^{13}C$. Throughout segment C, Re content increases from 0.69 to 15.05 ppb (Fig. 4). In segment D (122 to 81 m – middle part of C-isotope segment Ap3 to mid Ap7), Os_i values present overall stable values that range between 0.17 and 0.23. Segment D records stable unradiogenic Os_i values through a thick succession embracing most of the OAE 1a interval (upper part of the negative CIE, and the complete positive CIE), following up to the lower part of the Ap7 segment which postdates the OAE 1a. The top of this segment correlates with the FO of *E. floralis* (Figs. 4 and 6). At the base of D_1 segment (Fig. 4), ^{192}Os abundance increases from 54.7 to 508.0 ppt, and through the rest of D_1 segment, ^{192}Os remains high (~450 ppt), and Re content reaches a maximum of 29.63 ppb. The Os_i remains non-radiogenic below 0.2. Throughout Ap4 to the Lowest Occurrence (LO) of *E. floralis* (segments D_2 and D_3 – end of black shales – mid-Ap7; Fig. 4), the Os_i remains between 0.13 and 0.23, with elevated Re (5.8–22.3 ppb) and ^{192}Os (65.1–247.5 ppt). Segment E (Fig. 4) is defined from 81 to 55 m, which in the middle of Ap7, the Os_i reaches 0.60, then stays steady around 0.40 towards its top. Segment E extends for more than 1 Myr, with overall moderately non-radiogenic values, and records the transition to the upper Aptian, presenting the first Os_i result from the mid Ap7 to Ap10 C-isotope segments. This segment correlates with a gentle negative shift in C-isotope values, and its top lies within the *G. algerianus* biozone. Segment F (55 m to the top of the record – C-isotope segments mid-Ap10 to Ap14), defined here, is where the record Os_i values are slightly less unradiogenic than below, with a moderate upwards shift to more radiogenic (~0.50) values through the rest of the section. From the change in the Os_i to more radiogenic values in Ap7 (segments E and F), the Re content fluctuates between 0.43 and 9.61 ppb, whereas the ^{192}Os content remains relatively constant throughout the section (9.23 to 60.80 ppt), showing a slight decreasing-upwards trend. This segment correlates from the upper part of Ap10 to the base of Ap14 C-isotope segments, that record a basal negative peak followed by a gradual positive shift in C-isotope values, embracing the upper Aptian, from upper *G.algerianus* to *P. rohri* biozones.

We present and discuss the Re—Os data in terms of six segments, A to F (Fig. 5), although, based on the observed correlation with other Os_i profiles, we consider segment A to not be present at Cau.

5. Discussion

5.1. Os-isotope record

Os_i values give the best estimate of the $^{187}Os/^{188}Os$ composition of seawater during sedimentation, as demonstrated by the correlation with previous records of the OAE 1a interval (Bottini et al., 2012; Percival et al., 2021; Tejada et al., 2009;), as well as the good preservation of the C-isotope signal of the Cau core (Castro et al., 2021), which can rule-out a significant diagenetic overprint. Oscillations within the upper part of segment B_1, which coincide with similar oscillations in $\delta^{13}C$ and $\delta^{18}O$ and the presence of a fracture (or a fault) affecting the basal D4 segment likely favoured diagenetic fluids circulation, which finally produced an

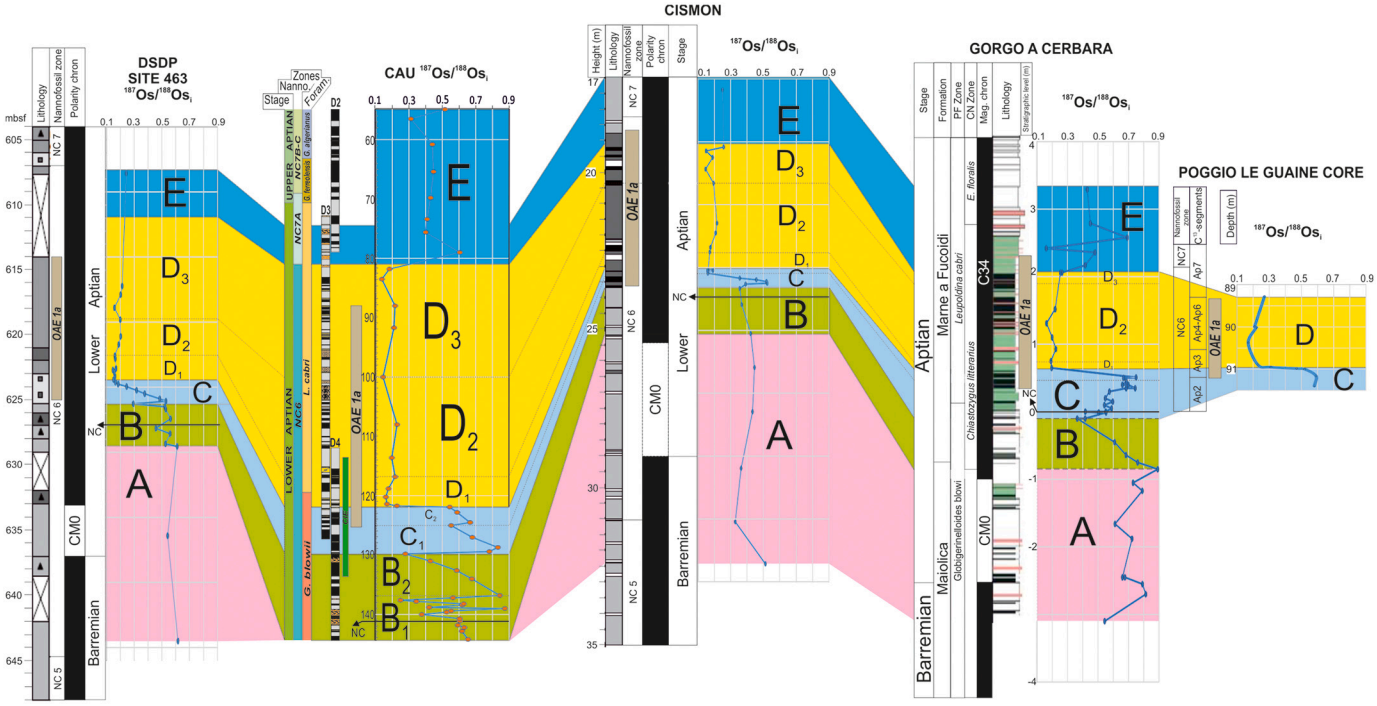

Fig. 5. Correlation of sections from DSDP Site 463 (mid Pacific Mountains, Pacific Ocean), Cau (southeastern Spain), Cismon (northern Italy), Gorgo a Cerbara (central Italy) and Poggio Le Guaine Core (Umbria-Marche basin, Italy) based on $^{187}Os/^{188}Os_i$ data (Data on Supplement 3).

alteration of the original geochemical signal. Nevertheless, these oscillations can reflect changes in the isotopic composition of the marine waters as discussed below. Alternatively, as Cau is an intra-shelf record sensitive to changes in sea-level, these short-lived changes in $\delta^{13}C$ and Os_i might be related to changes in sea-level (e.g., Du Vivier et al., 2015; Rooney et al., 2016; Jones et al., 2020), although no short-term relative sea level changes have been proposed in the Prebetic platform during the earliest Aptian (e.g., Castro et al., 2008; Martín-Chivelet et al., 2019).

5.1.1. Subsegment B_1

Prior to the onset of the major negative excursion in $\delta^{13}C$ that characterize the OAE 1a, the Os_i composition were moderately radiogenic between 0.6 and 0.7 (Fig. 4). Following the onset of the NC, the Os_i decrease to minimum values of 0.25 could reflect short-time inputs from unradiogenic sources (volcanic or cosmogenic), or a rapid decrease in the flux of radiogenic Os from continental weathering. As the studied sediments were deposited on a distal platform setting during an interval of dry climate conditions (e.g. Aguado et al., 2014a, 2014b), no significant changes in the continental weathering can be expected, nor cosmogenic sources have been reported for this interval; therefore they are considered to reflect pulses of volcanism from the early phases in the Ontong-Java plateau (e.g. Erba et al., 2015).

Interestingly, the onset of the NC coincides stratigraphically with the initiation of the $\delta^{13}C$ and Os_i fluctuations at 140.7 m depth. As the NC predates the onset of major LIP volcanism, no causal link can be established from our Os_i record. In this part of the record, other published sections show akin median Os_i values such as the Cismon section, a deeper water stratigraphic record, with Os_i values of ~0.45 (Segment A, Bottini et al., 2012) (Fig. 5), indicating open marine conditions (Rooney et al., 2016). In segment A, the Gorgo a Cerbara and DSDP Site 463 sections, with Os_i values of ~0.6–0.8 and ~ 0.6, respectively, do not show marked oscillations, which can be explained by the lower sampling resolution of these sections or the presence of a hiatus. Nevertheless, local factors at Cau (e.g. sea-level changes or diagenesis at this level) cannot be completely discarded. Further high-resolution Os_i records from other sites will aid in the interpretation of the Os_i data of the B_1 subsegment.

5.1.2. Subsegment B_2

Between 137 and 130 m (Os_i segment B_2, Fig. 4) a gradual shift in Os_i from 0.85 (radiogenic) to 0.30 (non-radiogenic) is observed. This trend in Os_i is interpreted to reflect a gradual increase in LIP magmatism yet could be explained by a 70% decrease in weathering (Tejada et al., 2009). This shift broadly correlates to the C-isotope transit Ap2a-b, which records the onset of the negative C-isotope excursion heralding the OAE 1a. This has been interpreted as the result of an input of C-13 depleted carbon into the atmosphere-ocean system (Castro et al., 2021; Méhay et al., 2009), and coincides with the beginning of an increase in atmospheric CO_2 level estimates from the Cau section (Naafs et al., 2016). This segment presents a record very similar to the Gorgo a Cerbara section (0.88 to 0.36; Tejada et al., 2009) (Fig. 5), and to DSDP Site 463 (0.6 to 0.3; Bottini et al., 2012) (Fig. 5). Cismon presents a lower resolution record but a slight decline in Os_i can be observed from 25 to 23.75 m (Os_i segment B, Fig. 5) (0.43 to 0.35). This volcanic pulse predates the OAE 1a by ca. 300 kyr (Bottini et al., 2012). Therefore, the Os_i data from Gorgo a Cerbara and Cau imply that the OJP LIP had an early pulse inducing a total increase of 60% of unradiogenic Os in the ocean (Tejada et al., 2009), predating the OAE 1a by 300–350 kyr (Fig. 6).

5.1.3. Segment C

From 130 to 129 m depth, there is a short-lived prominent shift to radiogenic Os_i, from 0.30 to 0.85, over a duration of ca. 50 kyr (Fig. 6). This excursion is also observed at Gorgo a Cerbara, Cismon and DSDP Site 463, which could indicate a global signal, related to a possible

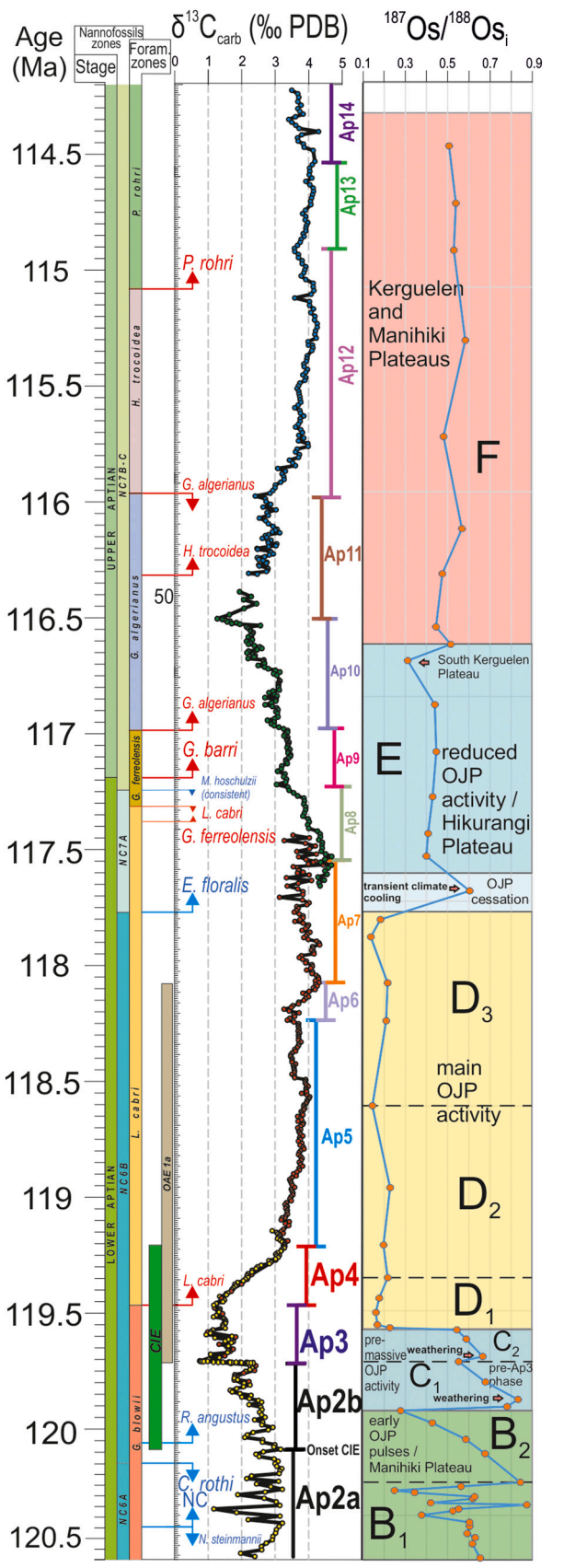

Fig. 6. Profiles of $\delta^{13}C$, and Os_i from the Cau Core, and possible volcanic sources during the Aptian.

abrupt cessation of the OJP activity and/or a rapid massive increase in global weathering rates (Tejada et al., 2009; Bottini et al., 2012). Although efficient oceanic circulation and mixing have been considered during this time interval (Bottini et al., 2012) given the similar timing of Os_i perturbations between the distanced sections of Cismon and DSDP Site 463, Cau is a shallower section, and chemical change of seawater signal could have arrived later to Cau. At DSDP Site 463, Cismon and Cau, this shift postdates the nannonconid crisis, whereas at Gorgo a Cerbara, the Os_i radiogenic excursion begins below the nannoconid crisis (Tejada et al., 2009). This could be related to a different mixing in the oceanic water, or a local continental input at this location. Nevertheless, differences in the definition or the record of the nannoconid crisis can not be ruled-out.

The rest of segment C is dominated generally by radiogenic values (>0.5 at Cau), interpreted as the result of increased weathering, probably linked to the activation of the hydrological cycle during the volcanic episode of segment B (Bottini et al., 2012). This is supported by the trend in Li-isotopes in this temporal interval at Resolution Guyot, Monte Raggeto, Santa Maria 4 core and Coppitella sections (Lechler et al., 2015), and also by Ca-isotopes at Resolution Guyot, Coppitella, and the English Chalk sections (Blättler et al., 2011). This enhanced weathering could have outpaced volcanism, although a decreased volcanic activity during segment C can not be discarded (Bottini et al., 2012). The Os_i record a double shift towards unradiogenic values trough this segment, probably indicating two pulses of volcanism, or alternatively one pulse punctuated with a brief period of enhanced weathering. This whole moderately radiogenic interval (129 to 122 m) correlates roughly with Cismon (23.5 m, Fig. 5) and Site 463 (625 mbsf, Fig. 5) sections, probably due to the expanded character of Cau. Nevertheless, the sharp radiogenic excursion in Os_i at both Cismon and Site 463 is indicating also the brief dominance of the radiogenic Os, which appears at the onset of the Selli Level equivalent (onset of the OAE 1a, Fig. 5) in the three sections.

Interestingly, the slight positive shift dividing the C segment coincides with a major negative spike in $\delta^{13}C$ values that marks the onset of OAE 1a. This negative excursion has been interpreted as evidence for the sudden addition of large quantities of isotopically light carbon from volcanic CO_2 sources and, possibly, from oxidized methane derived from gas hydrates (Adloff et al., 2020; Méhay et al., 2009; Weissert and Erba, 2004; Jahren et al., 2001) , or from marine organic-rich sediments in response to sill intrusions (Polteau et al., 2016). The high-resolution Os_i results at Cau are interpreted to indicate a punctual reduction of the volcanic activity during this C-isotope spike, and thus would point to an additional carbon source, possibly from oxizidez methane, during a short interval of <10 kyrs (Castro et al., 2021). This is consistent with a methane injection proposed by Erba et al. (2010), and maxima in temperatures at the onset of OAE 1a (Bottini et al., 2015; Naafs et al., 2016).

5.1.4. Segment D

An abrupt shift to non-radiogenic Os_i occurs at 122 m (0.53 to 0.16 over a thickness of 50 cm), which coincides with an elevated Re content and an abrupt increase in ^{192}Os content (from 54.70 to 508.01 ppt over a thickness of 50 cm, representing ca. 18 kyr). The segment extends from the middle part of the C-isotope segment Ap3 up to the mid part of the C-isotope segment Ap7, embracing most of the OAE 1a, and its top broadly coincides with the FO of *E. floralis*, postdating the OAE 1a, as defined by Ap3-Ap6 segments (e.g., Menegatti et al., 1998; Castro et al., 2021). The abrupt excursion to non-radiogenic Os_i is present in all published OAE 1a records (Fig. 5). Based on the sedimentation rate estimates for the Cau core (Castro et al., 2021), this Os_i excursion occurred ~75 ka after the onset of the OAE 1a. This delay between the onset of the OAE 1a and the onset of segment D is also observed in the Poggio Le Guaine Core section from the Umbria-Marche Basin (Percival et al., 2021). This abrupt non-radiogenic shift in Os_i and elevated ^{192}Os contents strongly suggests that Os was entering into the global ocean system due to mantle-related magmatism, and demonstrates that the peak volcanic activity of the OJP occurred after the onset of the OAE 1a. The base of the segment is also linked to a change in planktic foraminifera morphology, with the development of specimens showing elongated chambers. Such a morphological change suggests an adaptation to probable low-oxygen levels and to a perturbation in environmental conditions (in terms of temperature, salinity) (de Gea et al., 2003). Above its lower part, which coincides with the upper part of the C-isotope Ap3 segment, segment D corresponds to a long-lasting positive excursion in $\delta^{13}C$ values, considered to reflect widespread organic matter deposition in marine environments, in combination with increased continental weathering, leading to a reduction of ^{13}C-depleted carbon (e.g. Jenkyns, 2010; Castro et al., 2021).

Throughout segment D, the Os_i remain stable and non-radiogenic (0.14–0.20; Figs. 4, 7), thus continuing to be unradiogenic after the OAE 1a (lower part of the C-isotope segment Ap7). Similarly, at Gorgo a Cerbara and Poggio Le Guaine Core, values are ca. ~0.2 ($n = 8$ and 5 samples over 500 kyr and 1.5 m, respectively), whereas Cismon ($n = 13$ samples over 4 m) and DSDP Site 463 (n = 13 samples over 9.5 m) are between 0.15 and 0.20 (Fig. 5). Hence, this indicates continuous volcanic activity during the entire OAE 1a and postdating the OAE 1a (up to the middle part of C-isotope segment Ap7). The Os_i profile, clearly recorded in other sites with a strong similarity, confirms the global character of the non-radiogenic Os_i excursion, and an efficient ocean mixing at that time, probably favoured by global and local sea-level rise (Percival et al., 2021; Tejada et al., 2009; Bottini et al., 2012).

The prolonged non-radiogenic Os_i from Gorgo a Cerbara and Cismon (segment D) were used to suggest a duration for the main OJP magmatic of 1 Myr and ~ 880 kyr, respectively (Tejada et al., 2009; Bottini et al., 2012), as OJP main magmatic event was proposed to finish at the end of segment D. However, according to Cau core sedimentation rates, the duration of segment D is 1.3–1.6 Myr, an estimation longer than previously proposed. Yet, the main difference of the record of the Cau section with respect to other sections is that the end of segment D in Cau extensively postdates the OAE 1a, whereas in the other sections it ends at the same time as the OAE 1a or even before. Our results confirm that the main OJP activity continued after the OAE 1a, with the main phase of volcanism beginning ~50–150 kyr after the onset of the OAE 1a through to ca. 300 kyr after the end of the Selli Event.

5.1.5. Re and ^{192}Os in segment D

The segment D of the Cau core exhibit the highest abundances of Re and ^{192}Os, with the Ap4 segment showing the overall most significant enrichment (Fig. 4). Segment D_1 (122 to 117 m) shows the biggest increase in both Re and ^{192}Os in a double peak to 18 and 30 ppb, and to 508 and 448 ppt, respectively. A similar record is observed at the Cismon core, that displays a double peak in Re content (1 and 0.6 ppb) in the lowest part of the Selli Event (Fig. 7). The D_2 segment (117 to 100 m, Fig. 4) defined at Cau represents the middle part of the OAE 1a and presents a peak in Re and ^{192}Os of 23 ppb and 250 ppt, respectively (Fig. 4). Both the Gorgo a Cerbara and DSDP Site 463 sections present the main peak in Re and ^{192}Os content recorded within the middle part of the Selli Level (Fig. 7), and values return lower in the interval above. At Gorgo a Cerbara, however, a double ^{192}Os peak is observed that is not seen at Site 463, whereas Cismon is characterized, between 20.5 and 22.5 m, by minima in Re and ^{192}Os values (Fig. 7). Segment D_3 (100 to 81 m) encompasses the upper part of the OAE 1a and also presents a relatively high content in Re and ^{192}Os (Figs. 4, 7) similar to the record observed at Cismon between 19 and 20.5 m (Fig. 7). The similarity of data between sections with a different palaeosettings (Cau - intra-shelf record; Cismon - deep pelagic record; Gorgo a Cerbara - Western Tethys and DSDP Site 463 - Mid-Pacific Mountains) indicates an efficient marine circulation during the Selli Event.

5.1.6. Segment E

This segment extends over ca. 1.15 Myr following sedimentation rate estimates at Cau (Castro et al., 2021), recording the transition from the

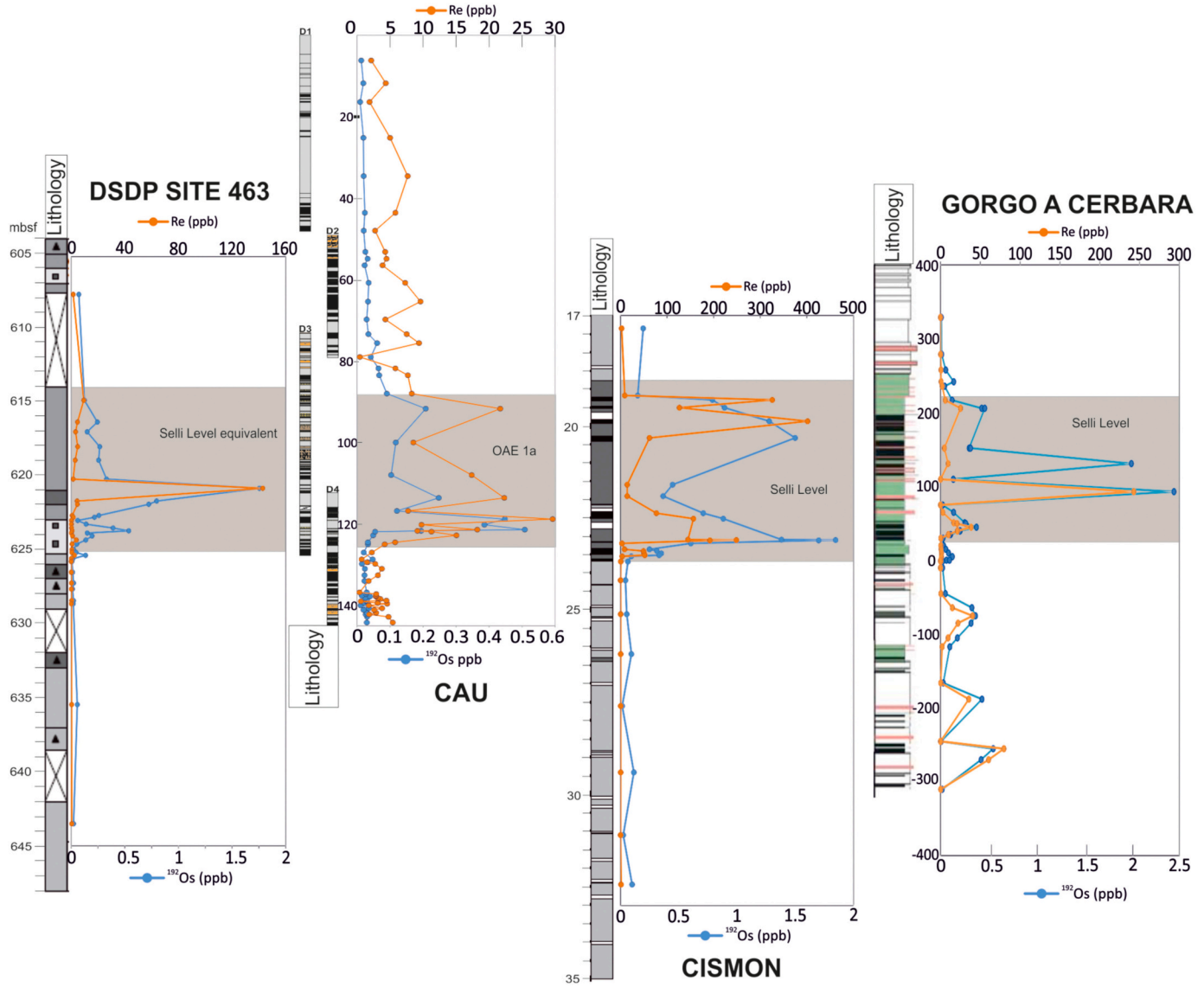

Fig. 7. ^{192}Os and Re profiles from the four sections correlated in this paper (they are showed in Fig. 5). The scale for Cau is different as it contains less quantity of Re and Os than the other three sections (Data on Supplement 3).

early to the late Aptian. The base of the segment is marked by a positive shift in Os_i from ca. 0.2 to 0.6 (Fig. 4). The Os_i values may reflect a cessation of the main OJP activity that led to a climate cooling from a reduction in CO_2 atmospheric concentrations postdating the OAE 1a. This is consistent with a coeval reduction in temperatures indicated by Tex_{86} and Nannofossil indices (McAnena et al., 2013; Aguado et al., 2014a; Bottini et al., 2015; Naafs and Pancost, 2016) as well as in CO_2 concentrations (Naafs et al., 2016), which discard a significant increase in weathering as an alternative explanation. This cooling episode would led to drier conditions and a subsequent reduction of the nutrient input to the ocean from the continent (Aguado et al., 2014a). A decrease of 3.8–5 °C in water surface temperatures favoured the recovery of the nannoconids (Bonin et al., 2016). TEX_{86} sea surface temperatures reconstruction (O'Brien et al., 2017) for the first third of the NC7 zone, that roughly corresponds to NC7A zone of Cau depicts a 1 °C increase in temperature from 31 to 32 °C, but the presence of the cold-water nannofossil species *E. floralis* not only in Cau, but globally (Bottini and Erba, 2018), is suggestive of cooler temperatures.

Only the base of segment E has been analyzed in previous Os_i studies. This Os_i record is similar to that at Gorgo a Cerbara (Fig. 5), that shows a shift up to 0.7 just before the recovery of the nannoconids (Fig. 5). Records at Cismon and DSDP Site 463 are very scarce (2 and 1 samples, respectively) and exhibit a relatively non-radiogenic Os_i composition (0.24–0.26). The Os_i data for Gorgo a Cerbara data supports our results, whereas values of Site 463 could be explained by its proximity to OJP, and the Cismon Os_i value could be related to an input of non-radiogenic Os derived from the weathering of ophiolites in the european hinterland (Peucker-Ehrenbrink and Ravizza, 2000; Kuroda et al., 2016), although more data would be necessary to confirm this hypothesis.

Overall, the Os_i values through the rest of Segment E remain steady around 0.4 with a gentle increase to 0.45 (Fig. 4). This interval records a reduced activity of the OJP and the initial spreading of the Hikurangi Plateau (HP, Figs. 1, 6). Feldspar $^{40}Ar/^{39}Ar$ dates of HP basement lavas that indicate an isochron age of 117.2 ± 4.7 Ma (Hoernle et al., 2010) are consistent with the chronology of this study. The pattern observed in this segment is likely related to a reduced but active volcanic activity, and considered to be responsible for the negative trend in C-isotopes, and the moderate warming (McAnena et al., 2013; Bottini et al., 2015). The generally cooler temperatures proposed for the upper part of segment E (C-isotope segments Ap8-Ap10) compared to the early Aptian, are not supportive of a period of enhanced weathering (McAnena et al., 2013; Erba et al., 2015; Castro et al., 2021). Yet,

interestingly, the hypothesis of gentle global warming is mirrored by Os_i records and increased TOC at Cau (maxima of 1.97%, Fig. 4), with could be interpreted to reflect volcanism resulting in a CO_2 concentration buildup, marking the transition between the early and the late Aptian. A similar evolution from minima to a moderate enrichment in other proxies (e.g., trace metals abundance) has been recognized during the early/late Aptian transition records from Cismon, DSDP Site 463 and DSDP Site 167 (Magellan Rise), which are interpreted to suggest a correlation between the degree of ocean oxygenation, LIP activity and primary productivity (Erba et al., 2015). The long negative excursion of C-isotope (Ap8 to Ap10) from ~5‰ to ~1‰ is double the magnitude of the onset of the OAE 1a, but the greater duration of the excursion is indicative of very different causative mechanism. Eventually, in the uppermost part of this segment, the Os_i low value of 0.31 (56.5 m, Figs. 4, 6) correlates with a moderately sharp negative pulse in C-isotopes (Ap10), which could reflect an initial pulse of submarine volcanism coming from the Southern Kerguelen plateau (SKP) (Coffin et al., 2002; Duncan, 2002; Frey et al., 2003). Sea-level estimations for this interval indicate a general high sea-level at Cau, with a notable sea-level drop in the upper part of the segment. Any relevant change in Os_i values or facies did occur, thus very likely during the lowstand interval, the sea-level was high enough to maintain an efficient water mixing.

5.1.7. Segment F

Finally, in segment F (C-isotope segments Ap11 to Ap14), Os_i values are steady at ~0.55, coming back to conditions near pre-OAE 1a (0.6–0.7) (segment F, Fig. 4). This part of the late Aptian, encompassing the upper part of *G. algerianus, H. trocoidea* and the lower part of *P. rohri*, is characterized by global climate cooling (McAnena et al., 2013). The Cau core Os_i values do not totally recover to pre-OAE 1a values. This observation implies the existence of a non-radiogenic source of Os. Consistent with the chronology of this study are the emergence of the Rajmahal Volcanic Province (Kerguelen Plateau, KP; Fig. 1) whose basalts present ^{40}Ar—^{39}Ar ages of 118–115 Ma (Kent et al., 2002; Ray et al., 2005), and the edifice construction of the Manihiki Plateau (Fig. 1) (Timm et al., 2011). In spite of the Kerguelen and Manihiki activity, which are indeed influencing the Os_i, the $\delta^{13}C$ seems unaffected by the LIP activity, describing a slow progression from ~2.5‰ to a steady ~4‰, indicating that the CO_2 consumption by continental weathering must have balanced the possible warming generated by the submarine oceanic plateaus. This seems a counterintuitive idea given the fact that some CO_2 estimations for this time interval depicts elevated atmospheric CO_2 (1200 to 1900 pppmV, Li et al., 2014). Nevertheless, the slower rate of increase in CO_2 concentration in comparison to the OAE 1a could account for a balance with continental weathering.

6. Conclusions

This study presents the first direct evidence that volcanic activity continued beyond the OAE 1a during the late Aptian. Our new Os-isotope data from the Cau Core confirm an extended time frame for the volcanic input of unradiogenic Os during the Aptian, likely due to emplacement of LIP and their continued activity, influencing composition of seawater Os for ~2.8 Myr.

The Cau Os_i data provide strong evidence to more accurately establish a high-resolution record of magmatic episodes and pulses of accelerated hydrological cycle, and exhibits the climatic instability that occurred before (Ap2 segment) and during the onset of the OAE 1a (Ap3 segment). This study confirms the temporal relationship of LIP magmatism with the OAE 1a, demonstrating that the magmatism was active 550–750 kyr prior to the Selli Event, was sustained through the entire OAE, and ceased ~300 kyr after the end of the event. The maximum duration calculated from the Os_i excursion linked to the main phase of the OJP is 1.6–1.75 Myr. Inference from the Os_i data suggests a minimum and maximum duration of LIP magmatism of 2.8 and 3.6 Myr.

The sequence of events recorded at Cau starts with a first volcanic pulse predating the OAE 1a, reflected in an abrupt negative shift in C-isotopes that may have been triggered by a pulse of methane emissions. This first event was followed by the main abrupt shift in non-radiogenic Os_i, followed by deposition of marine organic-rich sediments, indicating an increase in productivity and reduction of oxygenation due to the immense volcanism via CO_2 input, temperature increase and activation of hydrological cycle, resulting in nutrient-rich waters.

This record confirms the relation between the accumulation of organic matter, the development of anoxia/dysoxia and the productivity increase, with the initial pulses of volcanism that predate the main phase, as previously shown for other OAE 1a records (Tejada et al., 2009; Bottini et al., 2012).

During the late Aptian, the carbon cycle underwent a slow-paced change reflected in the long-term isotope excursion of the $\delta^{13}C$ record, although the Os_i record remained relatively stable, showing only punctual changes associated to volcanic pulses.

The expanded Aptian record at Cau highlights the different behaviour of the carbon cycle throughout the recorded time interval. In the early Aptian, the onset of the OAE 1a is associated with a rapid carbon negative isotope excursion produced in less than 25-kyr, which was followed by a strong change in the Os_i composition and perturbations recorded in multiple other proxies. In comparison, the negative carbon isotope excursion during the upper early Aptian-lower late Aptian transition, took place over a duration of ca. ~1 Myr, in which time, Os_i composition and other proxies remain stable. The delay between volcanic CO_2 outgassing in the ocean and enhanced continental weathering due to increased pCO_2 has to be considered when assessing different episodic pulses and the reflection of these changes in the $\delta^{13}C$ record.

Declaration of Competing Interest

The authors declare that they have no known competing financial interests or personal relationships that could have appeared to influence the work reported in this paper.

Acknowledgments

We greatly appreciate feedback from Emanuela Mattioli and from A. Godet that has improved this manuscript. Antonio Piedra, laboratory technician from University of Jaén, is thanked for assistance with sample preparation. We are grateful to Antonia Hofmann, Chris Ottley and Geoff Nowell for analytical support at Durham University. The visit of R. Martínez-Rodríguez to Durham was funded by a PhD-student grant from the University of Jaén. This work has been funded by the Spanish Government, Ministry of Science and Technology (research project CGL2014-55274-P), Research Group RNM-200 (Junta de Andalucía), and University of Jaén (FEDER-UJA 1265149). DS acknowledges the TOTAL endowment fund and the Dida Scholarship of CUG Wuhan. Dr. Lawrence Percival is also acknowledged for his helpful discussions on earlier stages of this work.

Appendix. Supplementary data

Supplementary data to this article can be found online at https://doi.org/10.1016/j.gloplacha.2021.103652.

References

Adloff, M., Green, S.E., Parkinson, I.J., Naafs, B.D.A., Preston, W., Ridgwell, A., Lunt, D. J., Castro, J.M., Monteiro, F., 2020. Unravelling the sources of carbon emissions at the onset of Oceanic Anoxic Event (OAE) 1a. Earth Planet. Sci. Lett. 530 (115947), 1–9. https://doi.org/10.1016/j.epsl.2019.115947.

Aguado, R., de Gea, G.A., Castro, J.M., O'Dogherty, L., Quijano, M.L., Naafs, B.D.A., Pancost, R.D., 2014a. Late Barremian–early Aptian dark facies of the Subbetic (Betic Cordillera, southern Spain): calcareous nannofossil quantitative analyses, chemostratigraphy and palaeoceanographic reconstructions. Palaeogeogr. Palaeoclimatol. Palaeoecol. 395, 198–221. https://doi.org/10.1016/j.palaeo.2013.12.031.

Aguado, R., de Gea, G.A., O'Dogherty, L., 2014b. Integrated biostratigraphy (calcareous nannofossils, planktonic foraminifera, and radiolaria) of an uppermost Barremian–lower Aptian pelagic succession in the Subbetic Basin (southern Spain). Cretac. Res. 51, 153–173. https://doi.org/10.1016/j.cretres.2014.06.002.

Aguado, R., Company, M., Castro, J.M., de Gea, G.A., Molina, J.M., Nieto, L.M., Ruiz-Ortiz, P.A., 2018. A new record of the Weissert episode from the Valanginian succession of Cehegín (Subbetic, SE Spain): bio-and carbon isotope stratigraphy. Cretac. Res. 92, 122–137. https://doi.org/10.1016/j.cretres.2018.07.010.

Allègre J., Claude, Luck, Jean-Marc, 1980. Osmium isotopes as petrogenetic and geological tracers. Earth and Planetary Science Letters 48 (1), 148–154. https://doi.org/10.1016/0012-821X(80)90177-6.

Arthur, M.A., Jenkyns, H.C., Brumsack, H.J., Schlanger, S.O., 1990. Stratigraphy, geochemistry and palaeoceanography of organic-carbon rich Cretaceous sequences. In: Ginsburg, R.N., Beaudoin, B. (Eds.), Cretaceous Resources, Events and Rhythms. Kluwer Academic Press, Dordrecht, Netherlands, pp. 75–119.

Bellanca, A., Erba, E., Neri, R., Premoli Silva, I., Sprovieri, M., Tremolada, F., Verga, D., 2002. Palaeoceanographic significance of the Tethyan 'Livello Selli' (early Aptian) from the Hybla Formation, northwestern Sicily: biostratigraphy and high-resolution chemostratigraphic records. Palaeogeogr. Palaeoclimatol. Palaeoecol. 185, 175–196.

Blakey, R.C., 2005. Palaeogeography and Geologic Evolution of North America: Images that Track the Ancient Landscapes of North America.

Blättler, Clara L., Jenkyns, Hugh C., Reynard, Linda M., Henderson, Gideon M., 2011. Calcium isotope composition of Oceanic Anoxic Events 1a and 2 sediments. PANGAEA. https://doi.org/10.1594/PANGAEA.786953. Supplement to: Blättler, CL et al. (2011): Significant increases in global weathering during Oceanic Anoxic Events 1a and 2 indicated by calcium isotopes. Earth and Planetary Science Letters, 309(1-2), 77-88, doi:10.1016/j.epsl.2011.06.029.

Bonin, A., Pucéat, E., Vennin, E., Mattioli, E., Aurell, M., Joachimski, M., Barbarin, N., Laffont, R., 2016. Cool episode and platform demise in the early Aptian: new insights on the links between climate and carbonate production. Palaeoceanography 31, 66–80. https://doi.org/10.1002/2015PA002835.

Bottini, C., Erba, E., 2018. Mid-cretaceous paleoenvironmental changes in the western Tethys. Clim. Past 14, 1147–1163. https://doi.org/10.5194/cp-14-1147-2018.

Bottini, C., Cohen, A.S., Erba, E., Jenkyns, H.C., Coe, A.L., 2012. Osmium isotope evidence for volcanism, weathering and ocean mixing during the early Aptian OAE 1a. Geology 40, 583–586. https://doi.org/10.1130/G33140.1.

Bottini, C., Erba, E., Tiraboschi, D., Jenkyns, H.C., Schouten, S., Sinninghe Damsté, J.S., 2015. Climate variability and ocean fertility during the Aptian Stage. Clim. Past 11 (3), 383–402. https://doi.org/10.5194/cp-11-383-2015.

Castro, J.M., de Gea, G.A., Ruiz-Ortiz, P.A., Nieto, L.M., 2008. Development of carbonate platforms on an extensional (rifted) margin. The Valanginian–Albian record of the Prebetic of Alicante (SE Spain). Cretac. Res. 29, 848–860. https://doi.org/10.1016/j.cretres.2008.05.012.

Castro, J.M., de Gea, G.A., Quijano, M.L., Aguado, R., Froehner, S., Naafs, B.D.A., Pancost, R.D., 2019. Complex and protracted environmental and ecological perturbations during OAE 1a-evidence from an expanded pelagic section from South Spain (Western Tethys). Glob. Planet. Chang. 103030.

Castro, J.M., Ruiz-Ortiz, Pedro A., de Gea, Ginés A., Aguado, Roque, Jarvis, Ian, Weissert, Helmut, Molina, José M., Nieto, Luis M., Pancost, Richard D., Quijano, María L., Reolid, Matías, Skelton, Peter W., López-Rodríguez, Carmina, Martínez-Rodríguez, Rafael, 2021. High-resolution C-isotope, TOC and biostratigraphic records of OAE1a (Aptian) from an expanded hemipelagic cored succession, Western Tethys: a new stratigraphic reference for global correlation and palaeoenvironmental reconstruction. Paleoceanogr. Paleoclimatol. 36 (3) https://doi.org/10.1029/2020PA004004.

Chandler, M.T., Wessel, P., Taylor, B., Seton, M., Kim, S.S., Hyeong, K., 2012. Reconstructing Ontong Java Nui: implications for Pacifi c absolute plate motion, hotspot drift and true polar wander. Earth Planet. Sci. Lett. 331, 140–151. https://doi.org/10.1016/j.epsl.2012.03.017.

Chumakov, N.M., Zharkov, M.A., Herman, A.B., Doludenko, M.P., Kalandadze, N.N., Lebedev, E.L., Ponomarenko, A.G., Rautian, A.S., 1995. Climatic belts of the mid-Cretaceous time. Stratigr. Geol. Correl. 3, 241–260.

Coffin, M.F., Pringle, M.S., Duncan, R.A., Gladczenko, T.P., Storey, M., Müller, R.D., Gahagan, L.A., 2002. Kerguelen hotspot magma output since 130 Ma. J. Petrol. 43, 1121–1137. https://doi.org/10.1093/petrology/43.7.1121.

de Gea, G.A., Castro, J.M., Aguado, R., Ruiz Ortiz, P.A., Company, M., 2003. Lower Aptian carbon-isotope stratigraphy from a distal carbonate shelf setting: the Cau section, Prebetic Zone, SE Spain. Palaeogeogr. Palaeoclimatol. Palaeoecol. 200, 207–219. https://doi.org/10.1016/S0031-0182(03)00451-6.

Duval, B., Brunet, M.F., Cadet, J.P., Crasquin, S., Sandulescu, M., 2000. In: Dercourt, J., Gaetani, M., Vrielynck, B., Barrier, E., Biju (Eds.), Atlas Peri-Tethys Palaeogeographical Maps. CCGM/CGMW, Paris, p. 268.

Du Vivier, A.D.C., Selby, D., Condon, D.J., Takashima, R., Nishi, H., 2015. Pacific 187Os/188Os isotope chemistry and U–Pb geochronology: synchroneity of global Os isotope change across OAE 2. Earth Planet. Sci. Lett. 428, 204–216.

Duncan, R.A., 2002. A time for construction of the Kerguelen Plateau and Broken Ridge. J. Petrol. 43, 1109–1119. https://doi.org/10.1093/petrology/43.7.1109.

Erba, E., 1994. Nannofossils and superplumes: the early Aptian "nannoconid crisis". Palaeoceanography 9, 483–501.

Erba, E., 2004. Calcareous nannofossils and Mesozoic oceanic anoxic events. Mar. Micropalaeontol. 52 (1–4), 85–106.

Erba, E., Tremolada, F., 2004. Nannofossil carbonate fluxes during the Early Cretaceous: phytoplankton response to nutrification episodes, atmospheric CO2 and anoxia. Palaeoceanography 19, 1–18.

Erba, E., Channell, J.E.T., Claps, M., Jones, C., Larson, R.L., Opdyke, B., Premoli Silva, I., Riva, A., Salvini, G., Torricelli, S., 1999. Integrated stratigraphy of the Cismon Apticore (Southern Alps, Italy): a "reference section" for the Barremian-Aptian interval at low latitudes. J. Foraminifer. Res. 29, 371–391.

Erba, E., Bottini, C., Weissert, J.H., Keller, C.E., 2010. Calcareous nannoplankton response to surface-water acidifi cation around Oceanic Anoxic Event 1a. Science 329, 428–432. https://doi.org/10.1126/science.1188886.

Erba, E., Duncan, R.A., Bottini, C., Tiraboschi, D., Weissert, H., Jenkyns, H.C., Malinverno, A., 2015. Environmental consequences of Ontong-Java Plateau and Kerguelen Plateau volcanism. In: Neal, C.R., Sager, W.W., Sano, T., Erba, E. (Eds.), The Origin, Evolution, and Environmental Impact of Oceanic Large Igneous Provinces, Geological Society of America Special Paper, Vol. 511, pp. 271–303. https://doi.org/10.1130/2015.2511(15).

Erbacher, J., Thurow, J., Littke, R., 1996. Evolution patterns of radiolarian and organic matter variations: a new approach to identify sea-level changes in mid-cretaceous pelagic environments. Geology 24, 499–502.

Frey, F.A., Coffin, M.F., Wallace, P.J., Quilty, P.J., 2003. Proceedings of the Ocean Drilling Program, Scientific Results, Vol. 183. Ocean Drilling Program, College Station, Texas. https://doi.org/10.2973/odp.proc.sr.183.015.2003.

Gradstein, F.M., Ogg, J.G., Schmitz, M.D., Ogg, G.M. (Eds.), 2020. The Geologic Time Scale 2020. Elsevier, Amsterdam, Netherlands.

Hay W., W., 2017. Toward understanding Cretaceous climate—An updated review. Science China Earth Sciences 60, 5–19. https://doi.org/10.1007/s11430-016-0095-9.

Herrle, et al., 2004. High-resolution carbon isotope records of the Aptian to Lower Albian from SE France and the Mazagan Plateau (DSDP site 545): A stratigraphic tool for paleoceanographic and paleobiologic reconstruction. Earth and Planetary Science Letters 218, 149–161. https://doi.org/10.1016/S0012-821X(03)00646-0.

Hoernle, K., Hauff, F., van den Bogaard, P., Werner, R., Mortimer, N., Geldmacher, J., Garbe-Schönberg, D., Davy, B., 2010. Age and geochemistry of volcanic rocks from the Hikurangi and Manihiki oceanic Plateaus. Geochim. Cosmochim. Acta 74, 7196–7219. https://doi.org/10.1016/j.gca.2010.09.030.

Jahren, A.H., Arens, N.C., Sarmiento, G., Guerrero, J., Amundson, R., 2001. Terrestrial record of methane hydrate dissociation in the early Cretaceous. Geology 29, 159–162. https://doi.org/10.1130/0091-7613(2001)029<0159:TROMHD>2.0.CO;2.

Jenkyns, H.C., 2003. Evidence for rapid climate change in the Mesozoic–Palaeogene greenhouse world. R. Soc. Lond. Philos. Trans. Ser A 361, 1885–1916. https://doi.org/10.1098/rsta.2003.1240.

Jenkyns, H.C., 2010. Geochemistry of oceanic anoxic events. Geochem. Geophys. Geosyst. 11, Q03004 https://doi.org/10.1029/2009GC002788.

Jones, C.E., Jenkyns, H.C., 2001. Seawater strontium isotopes, oceanic anoxic events, and seafloor hydrothermal activity in the Jurassic and Cretaceous. Am. J. Sci. 301, 112–149. https://doi.org/10.2475/ajs.301.2.112.

Jones, M.M., Sageman, Bradley B., Selby, David, Jicha, Brian R., Singer, Brad S., Titus, Alan L., 2020. Regional chronostratigraphic synthesis of the Cenomanian-Turonian Oceanic Anoxic Event 2 (OAE2) interval, Western Interior Basin (USA): new Re-Os chemostratigraphy and 40Ar/39Ar geochronology. GSA Bull. https://doi.org/10.1130/B35594.1.

Kent, R.W., Pringle, M.S., Muller, R.D., Saunders, A.D., Ghose, N.C., 2002. $^{40}Ar/^{39}Ar$ geochronology of the Rajmahal basalts, India and their relationship to the Kerguelen Plateau. J. Petrol. 43, 1141–1153.

Kerr, A.C., 1998. Oceanic plateau formation: a cause of mass extinction and black shale deposition around the Cenomanian–Turonian boundary. J. Geol. Soc. Lond. 155, 619–626.

Kuroda, J., Ogawa, N.O., Tanimizu, M., Coffin, M.F., Tokuyama, H., Kitazato, H., Ohkouchi, N., 2007. Contemporaneous massive subaerial volcanism and late cretaceous Oceanic Anoxic Event 2. Earth Planet. Sci. Lett. 256, 211–223.

Kuroda, J., Tanimizu, M., Hori, R.S., Suzuki, K., Ogawa, N.O., Tejada, M.L.G., Coffin, M. F., Coccioni, R., Erba, E., Ohkouchi, N., 2011. Lead isotopic record of Barremian–Aptian marine sediments: implications for large igneous provinces and the Aptian climatic crisis. Earth Planet. Sci. Lett. 307, 126–134. https://doi.org/10.1016/j.epsl.2011.04.021.

Kuroda, J., et al., 2016. Miocene to Pleistocene osmium isotopic records of the Mediterranean sediments. Paleoceanography 31, 148–166. https://doi.org/10.1002/2015PA002853.

Larson, R.L., Erba, E., 1999. Onset of the mid-Cretaceous greenhouse in the Barremian–Aptian: Igneous events and the biological, sedimentary and geochemical responses. Palaeoceanography 14, 663–678. https://doi.org/10.1029/1999PA900040.

Lechler, M., Strandmann, P.A.E.P., Jenkyns, Hugh, Prosser, Giacomo, Parente, Mariano, 2015. Lithium-isotope evidence for enhanced silicate weathering during OAE 1a (early Aptian Selli Event). Earth Planet. Sci. Lett. 432, 210–222.

Leckie, R.M., Bralower, T.J., Cashman, R., 2002. Oceanic anoxic events and plankton evolution: biotic response to tectonic forcing during the mid-cretaceous. Palaeoceanography 17, 13–29.

Li, X., Jenkyns, H.C., Zhang, C., Wang, Y., Liu, L., Cao, K., 2014. Carbon isotope signatures changes during middle- of pedogenic carbonates from SE China: rapid atmospheric pCO2 late early Cretaceous time. Geol. Mag. 151, 830–849.

Lorenzen, J., Kuhnt, W., Holbourn, A., Flögel, S., Moullade, M., Tronchetti, G., 2013. A new sediment core from the Bedoulian (Lower Aptian) stratotype at Roquefort–La Bédoule, SE France. Cretaceous Research 39, 6–16. https://doi.org/10.1016/j.cretres.2012.03.019.

Mahoney, J., Fitton, G., Wallace, P., 2001. ODP Leg 192: Basement drilling on the Ontong Java Plateau. JOIDES Journal 27 (2), 2–6.

Malinverno, A., Erba, E., Herbert, T.D., 2010. Orbital tuning as an inverse problem: chronology of the early Aptian oceanic anoxic event 1a (Selli Level) in the Cismon

APTICORE. Palaeoceanography 25. https://doi.org/10.1029/2009PA001769. PA2203.
Malinverno, A., Hildebrandt, J., Tominaga, M., Channell, J.E.T., 2012. M-sequence geomagnetic polarity time scale (MHTC12) that steadies global spreading rates and incorporates astrochronology constraints. J. Geophys. Res. 117, B06104 https://doi.org/10.1029/2012JB009260.
Martín-Chivelet, J., Berasategui, X., Rosales, I., Vilas, L., Vera, J.A., Caus, E., Gráfe, K.U., Mas, R., Puig, C., Segura, M., Robles, S., Floquet, M., Quesada, S., Ruiz-Ortiz, P.A., Frenegal-Martínez, M.A., Salas, R., García, A., Martín-Algarra, A., Arias, C., Meléndez, M., Chacón, B., Molina, J.M., Sanz, J.L., Castro, J.M., García-Hernández, M., Carenas, B., García-Hidalgo, J., Gil, J., Ortega, F., 2002. Cretaceous. In: Gibbons, W., Moreno, T. (Eds.), The Geology of Spain. The Geological Society, London, UK.
Martín-Chivelet, J., López-Gómez, J., Aguado, R., Arias, C., Arribas, J., Arribas, M.E., Aurell, M., Bádenas, B., Benito, M.I., Bover-Arnal, T., Casas-Sainz, A., Castro, J.M., Coruña, F., de Gea, G.A., Fornós, J.J., Fregenal-Martínez, M., García-Senz, J., Garófano, D., Gelabert, B., Giménez, J., González-Acebrón, L., Guimerà, J., Liesa, C. L., Mas, R., Meléndez, N., Molina, J.M., Muñoz, J.A., Navarrete, R., Nebot, M., Nieto, L.M., Omodeo-Salé, S., Pedrera, A., Peropadre, C., Quijada, I.E., Quijano, M.L., Reolid, M., Robador, A., Rodríguez-López, J.P., Rodríguez-Perea, A., Rosales, I., Ruiz-Ortiz, P.A., Sàbat, F., Salas, R., Soria, A.R., Suarez-Gonzalez, P., Vilas, L., 2019. The late Jurassic – early cretaceous rifting. In: Quesada, C., Oliveira, J.T. (Eds.), The Geology of Iberia: A Geodynamic Approach. Regional Geology Reviews. Springer, Cham, 1023 Switzerland. https://doi.org/10.1007/978-3-030-11295-0_5.
Martinez, M., Aguado, R., Company, M., Sandoval, J., O'Dogherty, L., 2020. Integrated astrochronology of the Barremian Stage (early Cretaceous) and its biostratigraphic subdivisions. Glob. Planet. Chang. 195, 103368. ISSN 0921-8181. https://doi.org/10.1016/j.gloplacha.2020.103368.
Masse, J.P., Bellion, Y., Benkhelil, J., Boulin, J., Cornee, J.J., Dercourt, J., Guiraud, R., Mascle, G., Poisson, A., Ricou, L.E., Sandulescu, M., 1993. Lower Aptian palaeoenvironments 114–112 Ma. In: Dercourt, J., Ricou, L.E., Vrielynck, B. (Eds.), Atlas Tethys Palaeoenvironmental Maps. BEICIP- FRANLAB, Rueil-Malmaison, France.
Matsumoto, H., Kuroda, J., Coccioni, R., et al., 2020. Marine Os isotopic evidence for multiple volcanic episodes during Cretaceous Oceanic Anoxic Event 1b. Sci. Rep. 10, 12601. https://doi.org/10.1038/s41598-020-69505-x.
McAnena, A., Flögel, S., Hofmann, P., Herrle, J.O., Griesand, A., Pross, J., Talbot, H.M., Rethemeyer, J., Wallmann, K., Wagner, T., 2013. Atlantic cooling associated with a marine biotic crisis during the mid-Cretaceous period. Nat. Geosci. 6, 558–561. https://doi.org/10.1038/ngeo1850.
Méhay, S., Keller, C.E., Bernasconi, S.M., Weissert, H., Erba, E., Bottini, C., Hochuli, P.A., 2009. A volcanic CO2 pulse triggered the Cretaceous Oceanic Anoxic Event 1a and a biocalcification crisis. Geology 37, 819–822. https://doi.org/10.1130/G30100A.1.
Melinte, M., Mutterlose, J., 2001. A Valanginian (early Cretaceous) 'boreal nannoplankton excursion' in sections from Romania. Mar. Micropalaeont. 43, 1–25.
Menegatti, A.P., Weissert, H., Brown, R.S., Tyson, R.V., Farrimond, P., Strasser, A., Caron, M., 1998. High-resolution δ13C stratigraphy through the early Aptian "Livello Selli" of the Alpine Tethys. Palaeoceanography 13, 530–545. https://doi.org/10.1029/98PA01793.
Misumi, K., Yamanaka, Y., 2008. Ocean anoxic events in the mid-Cretaceous simulated by a 3-D biogeochemical general circulation model. Cretac. Res. 29, 893–900.
Naafs, B.D.A., Pancost, R.D., 2016. Sea-surface temperature evolution across Aptian Oceanic Anoxic Event 1a. Geology 44, 959–962. https://doi.org/10.1130/G38575.1.
Naafs, B.D.A., Castro, J.A., De Gea, G.A., Quijano, M.L., Schmidt, D.N., Pancost, R.D., 2016. Gradual and sustained carbon dioxide release during Aptian oceanic anoxic event 1a. Nat. Geosci. 9, 135–139. https://doi.org/10.1038/ngeo2627.
Neal, C.R., Coffin, M.F., Arndt, N.T., Duncan, R.A., Eldholm, O., Erba, E., Farnetani, C., Fitton, J.G., Ingle, S.P., Ohkouchi, N., Rampino, M.R., Reichow, M.K., Self, S., Tatsumi, Y., 2008. Investigating large igneous province formation and associated palaeoenvironmental events: a white paper for scientific drilling. Sci. Drill. (6), 4–18. https://doi.org/10.2204/iodp.sd.6.01.2008.
O'Brien, C.L., Robinson, S.A., Pancost, R.D., Damsté, J.S.S., Schouten, S., Lunt, D.J., Alsenz, H., Bornemann, A., Bottini, C., Brassell, S.C., Farnsworth, A., Forster, A., Huber, B.T., Inglis, G.N., Jenkyns, H.C., Linnert, C., Littler, K., Markwick, P., McAnena, A., Mutterlose, J., Naafs, B.D.A., Püttmann, W., Sluijs, A., van Helmond, A.G.M., Vellecoop, J., Wagner, T., Wrobel, N.E., 2017. Cretaceous sea-surface temperature evolution: constraints from TEX_{86} and planktonic foraminiferal oxygen isotopes. Earth-Sci. Rev. 172 (224–247), 2017.
Olierook, H.J.H., Jourdan, F., Merle, R.E., 2019. Age of the Barremian–Aptian boundary and 1069 onset of the Cretaceous Normal Superchron. Earth Sci. Rev. 197, 102906. https://doi.org/10.1016/j.earscirev.2019.102906.
Percival, L., Tedeschi, L., Creaser, R., Bottini, C., Erba, E., Giraud, F., Svensen, H., Savian, J., Trindade, R., Coccioni, R., Frontalini, F., Jovane, L., Mather, T.A., Jenkyns, H., 2021. Determining the style and provenance of magmatic activity during the Early Aptian Oceanic Anoxic Event (OAE 1a). Global and Planetary Change 200. https://doi.org/10.1016/j.gloplacha.2021.103461.
Peucker-Ehrenbrink, B., Ravizza, G., 2000. The marine osmium isotope record. Terra Nova 12, 205–219. https://doi.org/10.1046/j.1365-3121.2000.00295.x.
Polteau, S., Hendriks, B.W., Planke, S., Ganerød, M., Corfu, F., Faleide, J.I., Midtkandal, I., SvensenHS, Myklebust R., 2016. The early Cretaceous Barents Sea Sill Complex: distribution, 40Ar/39Ar geochronology, and implications for carbon gas formation. Palaeogeogr. Palaeoclimatol. Palaeoecol. 441, 83–95. https://doi.org/10.1016/j.palaeo.2015.07.007.
Ray, J.S., Pattanayak, S.K., Pande, K., 2005. Rapid emplacement of the Kerguelen plume-related Sylhet Traps, eastern India: evidence from $^{40}Ar-^{39}Ar$ geochronology. Geophys. Res. Lett. 32, 1–4.
Rooney, A.D., Selby, David, Lloyd, Jeremy M., Roberts, David H., Lückge, Andreas, Sageman, Bradley B., Prouty, Nancy G., 2016. Tracking millennial-scale Holocene glacial advance and retreat using osmium isotopes: insights from the Greenland ice sheet. Quat. Sci. Rev. 138, 49–61. ISSN 0277-3791. https://doi.org/10.1016/j.quascirev.2016.02.021.
Ruiz-Ortiz, P.A., 2010. Contribución al conocimiento de las zonas externas de la Cordillera Bética a lo largo de 30 años de investigación geológica: *Discurso de Ingreso en el Instituto de Estudios Giennenses*. Diputación Provincial de Jaén, 96 p.
Schlanger, S.O., Jenkyns, H.C., 1976. Cretaceous oceanic anoxic events: causes and consequences. Neth. J. Geosci. Geol. Mijnbouw 55, 179–184 (Classic Papers).
Selby, David, Creaser, Robert, 2003. Re-Os geochronology of organic rich sediments: an evaluation of organic matter analysis methods. Chem. Geol. 200, 225–240. https://doi.org/10.1016/S0009-2541(03)00199-2.
Skelton, P.W. (Ed.), 2003. The Cretaceous World. Cambridge University Press and The Open University, Cambridge, UK.
Skelton, P.W., Gili, E., 2012. Rudists and carbonate platforms in the Aptian: a case study on biotic interactions with ocean chemistry and climate. Sedimentology 59, 81–117. https://doi.org/10.1111/j.1365-3091.2011.01292.x.
Skelton, P.W., Castro, J.M., Ruiz-Ortiz, P.A., 2019. Aptian carbonate platform development in the Southern Iberian Palaeomargin (Prebetic of Alicante, SE Spain). BSGF - Earth Sci. Bull. 190, 3. https://doi.org/10.1051/bsgf/2019001.
Smoliar, M.I., Walker, R.J., Morgan, J.W., 1996. Re-Os ages of group IIA, IIIA, IVA, and IVB iron meteorites. Science 271 (5252), 1099–1102.
Snow, L.J., Duncan, R.A., Bralower, T.J., 2005. Trace element abundances in the Rock Canyon Anticline, Pueblo, Colorado, marine sedimentary section and their relationship to Caribbean plateau construction and oxygen anoxic event 2. Palaeoceanography 20, PA3005. https://doi.org/10.1029/2004PA001093.
Tarduno, J.A., Sliter, W.V., Kroenke, L., Leckie, M., Mayer, H., Mahoney, J.J., Musgrave, R., Storey, M., Winterer, E.L., 1991. Rapid formation of Ontong Java Plateau by Aptian mantle plume volcanism. Science 254 (5030), 399–403. https://doi.org/10.1126/science.254.5030.399.
Taylor, Brian, 2006. The single largest oceanic plateau: Ontong Java–Manihiki–Hikurangi. Earth and Planetary Science Letters 241 (3–4), 372–380. https://doi.org/10.1016/j.epsl.2005.11.049.
Tejada, M.L.G., Suzuki, K., Kuroda, J., Coccioni, R., Mahoney, J.J., Ohkouchi, N., Tatsumi, Y., 2009. Ontong-Java Plateau eruption as a trigger for the early Aptian oceanic anoxic event. Geology 37, 855–858. https://doi.org/10.1130/G25763A.1.
Timm, C., Hoernle, K., Werner, R., Hauff, F., van den Bogaard, P., Michael, P., Coffin, M. F., Koppers, A., 2011. Age and geochemistry of the oceanic Manihiki Plateau, SW Pacific: new evidence for a plume origin. Earth Planet. Sci. Lett. 304, 135–146. https://doi.org/10.1016/j.epsl.2011.01.025.
Turgeon, S.C., Creaser, R.A., 2008. Cretaceous oceanic anoxic event 2 triggered by a massive magmatic episode. Nature 454, 323–326.
van Breugel, Y., Schouten, S., Tsikos, H., Erba, E., Price, G.D., Sinninghe Damsté, J.S., 2007. Synchronous negative carbon isotope shifts in marine and terrestrial biomarkers at the onset of the early Aptian oceanic anoxic event 1a: evidence for the release of 13C-depleted carbon into the atmosphere. Palaeoceanography 22, PA1210. https://doi.org/10.1029/2006pa001341.
Vera, J.A. (Coord.), 2004. Cordillera Bética y Baleares. In: Vera, J.A. (Ed.), Geología de España. Sociedad Geológica de España & Instituto Geológico y Minero de España, Madrid, Spain.
Weissert, H., Bréheret, J.G., 1991. A carbonate-isotope record from Aptian-Albian sediments of the Vocontian Trought (SE France). Bull. Soc. Géol. France 162, 1133–1140.
Weissert, H., Erba, E., 2004. Volcanism, CO2 and palaeoclimate: A Late Jurassic–Early Cretaceous carbon and oxygen isotope record. Journal of the Geological Society 161, 695–702. https://doi.org/10.1144/0016-764903-087.
Weissert, H., Lini, A., Föllmi, K.B., Kuhn, O., 1998. Correlation of cretaceous carbon isotope stratigraphy and platform drowning events: a posible link? Palaeogeogr. Palaeoclimatol. Palaeoecol. 137, 189–203.